TOPICAL REVIEW — Iron-based high temperature superconductors

Photoemission study of iron-based superconductor*

Liu Zhong-Hao(刘中灏), Cai Yi-Peng(蔡贻鹏), Zhao Yan-Ge(赵彦阁),
Jia Lei-Lei(贾雷雷), and Wang Shan-Cai(王善才)†

Department of Physics, Renmin University of China, Beijing 100872, *China*

(Received 16 June 2013; revised manuscript received 24 June 2013)

The iron-based superconductivity (IBSC) is a great challenge in correlated system. Angle-resolved photoemission spectroscopy (ARPES) provides electronic structure of the IBSCs, the pairing strength, and the order parameter symmetry. Here, we briefly review the recent progress in IBSCs and focus on the results from ARPES. The ARPES study shows the electronic structure of "122", "111", "11", and "122*" families of IBSCs. It has been agreed that the IBSCs are unconventional superconductors in strong coupling region. The order parameter symmetry basically follows $s_{\pm}$ form with considerable out-of-plane contribution.

Keywords: iron-based superconductor, angle-resolved photoemission spectroscopy, gap, pairing symmetry

PACS: 74.25.Jb, 74.20.–z, 74.20.Rp, 74.25.–q **DOI:** 10.1088/1674-1056/22/8/087406

1. Introduction

The discovery of iron based superconductivity with highest $T_C \sim 55$ K in 2008 has aroused the great interest in understanding the superconductivity in this material.[1,2] It brought a wonderful chance in studying the mechanism of high T_C superconductivity. The iron-based superconductivity (IBSC) is another family of unconventional superconductors with transition temperature above the McMillan limit besides the cuprate superconductors, where the superconductivity cannot be described by a weak coupling BCS theory. The cuprate superconductors had been the center of the study of high temperature superconductivity and extensively studied for more than twenty years. However, no consensus on the mechanism of superconductivity has been reached, partially due to the uniqueness of cuprates in high T_C superconductivity. Thus the IBSCs bring a chance in studying the unconventional superconductivity in comparison with the cuprate superconductors.

The electronic structures of cuprate superconductors and the IBSCs are different. The cuprate superconductor evolves from a doped Mott insulator where the strong electron–electron correlation dominates. The Cu–O plane contributes most to the electronic structure at Fermi energy, and a single Fermi-surface is observed for this material. The parent compounds of IBSCs are semi-metal, five bands from the Fe–As layer are present at the Fermi level. The electron–electron correlation may not be as important as that in cuprate superconductor.

From structure point of view, there are four major families of IBSCs intensively studied by different techniques. All families each have an essential building block of FeAs or FeSe layers which are separated by the intercalation layers. Based on the structure and chemical compositions, they are classified as "1111", "122", "111", and "11" families respectively. Recently, a new "122*" type was discovered with T_C up to 44 K,[3] whose structure in superconducting phase is still under debate. The FeAs layer contributes most to the electronic properties near the Fermi energy (E_F) in iron-pnictides, while the FeSe layer contributes most in "11" and "122*" types.

Most of the IBSCs have similar phase diagrams. Most parent compounds are semi-metals with antiferromagnetic (AFM) magnetic ordered ground states. By introducing a dopant or chemical substitution, the IBSC evolves into the superconducting state, while it may undergo structural and magnetic transitions.[4,5] The doping or chemical substitution could be at the FeAs layer, e.g., $Ba(Fe_{1-x}Co_x)_2As_2$ and $BaFe_2As_{1-x}P_x$, or out of the FeAs plane, e.g. $Ba_{1-x}K_xFe_2As_2$. Owing to the complexity of the IBSCs, the phase diagrams of different families are not unified yet. The parent compounds of "1111" and "122" families have SDW ground states, while in the "111"-type's parent compound the SDW is very weak or totally absent.[5,6]

Angle-resolved photoemission spectroscopy (ARPES) is a powerful tool in studying the electronic structure of the IBSC. It is a unique technique in probing the momentum and energy distribution of the outgoing electron simultaneously. It can probe the electronic structure of system such as band dispersion, superconducting gaps, gap symmetry, etc.

The electronic structures are very analogous in all IBSCs. Based on the LDA calculation and ARPES observations, the Fe 3d orbitals are the dominant feature at E_F. Three hole-like

*Project supported by the National Natural Science Foundation of China (Grant No. 11274381) and the National Basic Research Program of China (Grant No. 2010CB923000).

†Corresponding author. E-mail: scw@ruc.edu.cn

© 2013 Chinese Physical Society and IOP Publishing Ltd

bands are observed at the Brillouin Zone (BZ) center and two electron-like bands at the BZ corner. The bands in IBSC show more three-dimensional (3D) features than those in cuprate superconductor, the band dispersion along the c axis in IBSCs is stronger, especially for the hole band in the BZ center.

In the superconducting state, the superconducting gaps open at all FSs. The gap size is different for different FS and is momentum dependent. The gap symmetry can be described by an $s_{\pm}$ formula with considerable c-axis variation. From the observation of the FS topology, an inter-FS scattering induced pairing mechanism has been proposed, and an $s_{\pm}$ form of pairing symmetry is observed at most IBSCs. However, a great challenge occurs from the "122*" type $A_{2-y}Fe_xSe_2$ (A = K, Rb, Tl, etc.) where the FSs of hole-like bands near BZ center are absent. Thus, a local pairing scenario was proposed to understand the pairing symmetry, however, no consensus on the pairing mechanism on the IBSCs has been reached so far.

2. Crystal structure

The structures of the IBSCs at room temperature are shown in Fig. 1. All IBSCs have tetragonal structures with common FeAs or FeSe layers stacking along the c axis as shown in the figure. The Fe^{2+} ions in FeAs layer form a square-planar sheet and are bridged by the off-plane As/Se ions. The bridging As/Se has two positions, alternatively above and below the Fe-square sheet. Two Fe atoms per unit cell are used in ARPES, albeit the LDA calculation prefers one Fe atom per unit cell by ignoring the bridging As/Se. In the following discussion, two Fe atoms per unit cell are used unless otherwise stated. The parent compounds are non-superconducting for most IBSCs, when a dopant or substitution is introduced, it could be either in-plane doping as $LaFeAsO_{1-x}F_x$, $BaFe_{2-x}Co_xAs_2$, or in the intercalation plane as $Ba_{1-x}K_xFe_2As_2$.

Typical phase diagrams of "122" and "111" iron-pnictides are shown in Fig. 2. The parent compounds have collinear magnetic structures at low temperature due to the AFM interaction. Transport measurement suggested a spin density wave (SDW) state as the ground state. When cooling down from the room temperature to the SDW state for low doping levels, the materials experience a structural and magnetic transition from the tetrahedral into the orthorhombic structure and the SDW state. Upon doping, the transition temperature decreases and the superconducting transition temperature increases. In the low doping region, the "122" and "111" each have the coexistence between SDW and superconductivity.[8] It is noteworthy that for undoped NaFeAs, there exists a diamagnetic signal at low temperature, indicating the coexistence of superconducting and SDW phase.[9] The optimum T_C occurs in an intermediate doping region and the T_C line has a doom shape.

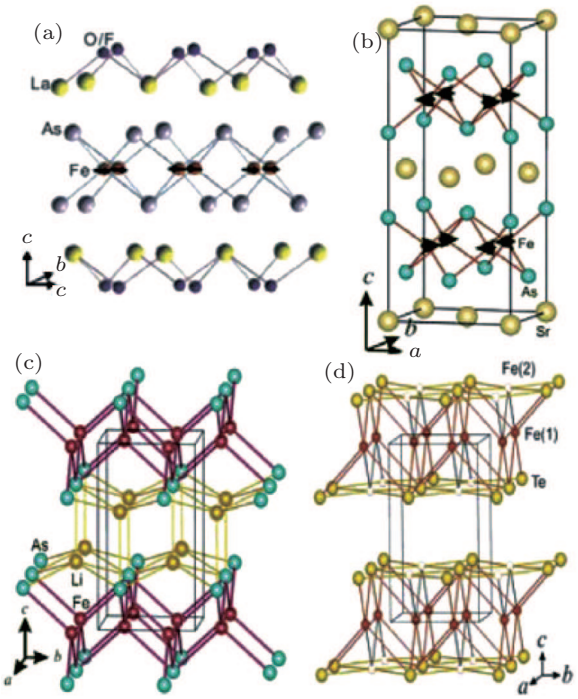


Fig. 1. The crystal structures of the four classes of superconductors: (a) LaFeAsO (1111), (b) $SrFe_2As_2$ (122), (c) LiFeAs (111), and (d) $Fe_{1+x}Te$ (11). Cited from Ref. [7].

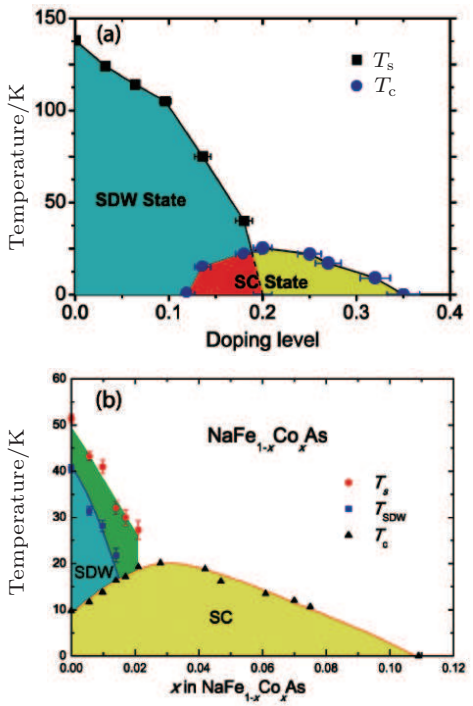


Fig. 2. Phase diagram of (a) electron doped "122"-type $BaFe_{2-x}Co_xAs_2$ and (b) "111"-type $NaFe_{1-x}Co_xAs$. Panel (a) is cited from Ref. [8]. Panel (b) is cited from Ref. [9].

3. Angle-resolved photoemission spectroscopy

ARPES is a unique technique in directly probing the electronic structure of materials. It is based on the photoelectric

effect that a photon shines on the sample and will be absorbed by the electron inside material and the excited electrons escaping from material will carry the information in the band. A sketch of the ARPES experiment is shown in Fig. 3. When an incident photon with energy $h\nu$ is absorbed by an electron inside the material, the energy and momentum of the outgoing electrons are directly connected to the electron inside the solid by the conservation of energy and momentum

$$E_{\rm kin} = h\nu - \phi - E_{\rm B}, \quad (1)$$

$$k_{\parallel} = k_{\parallel,\rm inside}. \quad (2)$$

A detector collects outgoing electrons and identifies the kinetic energy $E_{\rm kin}$, and the momentum parallel to the surface is calculated by $k_{\parallel} = \sqrt{2m_{\rm e}E_{\rm kin}/\hbar^2}\sin\theta$. The momentum perpendicular to the surface is not conserved but could be estimated by

$$k_{\perp} = \frac{1}{\hbar}\sqrt{2m_{\rm e}(h\nu - \phi - E_{\rm B} + V_0) - \hbar^2 k_{\parallel}^2},$$

where the V_0 is the inner potential which could be determined empirically.

The detector signal $I(k,\omega,\boldsymbol{A},h\nu)$ could be simplified into the product of three parts, the matrix elements $I_0(\boldsymbol{A},h\nu)$, the Fermi–Dirac distribution $f(\omega,T)$, and the spectral function $A(k,\omega)$

$$I(k,\omega,A,h\nu) = I_0(A,h\nu)\cdot A(k,\omega)\cdot f(\omega,T),$$

where $A(k,\omega)$ is the one-particle spectral function which is the imaginary part of the Green's function. From the spectral function, we can extract the information about band dispersion, determine the Fermi surface topology, and study the superconducting gap and the self-energy of correlated electrons. The Fermi–Dirac distribution $f(\omega,T) = 1/(\mathrm{e}^{\omega/k_{\rm B}T}+1)$ limits the spectrum to the occupied side of the electron state. The matrix element $I_0(\boldsymbol{A},h\nu)$ is a prefactor, which is ignored most of the time, determined by the experimental geometry. A certain band intensity could be fully suppressed or greatly enhanced in the mirror plane if the electric field vector of the incident photon lies in or is perpendicular to the mirror plane. The matrix elements are mostly used to determine the band parity with respect to the mirror plane and analyze the orbital origin in the IBSC.

The ARPES spectrum $A(k,\omega)$ is the imaginary part of the Green's function. The lineshape is an ultra-sharp quasiparticle peak in energy and momentum space for a non-interacting particle. When the electron interaction is switched on or an electron is coupled with other modes, the electron's self-energy correction will cause the spectrum to broaden and the band dispersion will also be affected. The linewidth analysis and dispersion will give the information about electron–electron interaction and the coupling strength of electron and modes. ARPES provides a direct measure of the self-energy and electron-excitation interaction.[11]

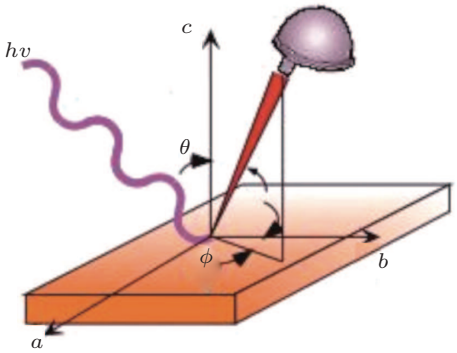


Fig. 3. Schematic diagram of ARPES experiment. A flux of photon with energy $h\nu$ shines on the sample. The outgoing photoelectron with kinetic energy $E_{\rm kin}$ escaping at the angle (θ, ϕ) is detected by the electron analyzer. In the process, the momentum parallel to the surface is conserved.

The ARPES experiment is a surface sensitive technique due to the short electron escape length. For a typical photon energy used for ultraviolet photoemission, $h\nu$ in a 10-eV–100-eV range, the escape length is less than a nanometer which is approximately the lattice constant c of the superconducting material. The contribution from the surface state is not negligible in most cases. An assumption that the electronic structure at the surface is bulk representative, is needed, but the caution should be taken about the existence of surface state. During the experiment, the ultra-high vacuum is maintained to keep the cleaved surface from being contaminated. On the other hand, being surface-sensitive makes ARPES an ideal technique in studying the surface related phenomenon, like topological insulator.[12]

4. Electronic structure of iron-based superconductor

For ARPES study of IBSCs, the samples are cleaved *in situ* for photoemission measurement. After cleavage, the exposed top layer could be an FeAs layer, an intercalating layer, or the mixture of both. Owing to the asymmetry of the cleaved surfaces in "1111" and "122" families, the termination layer will not be unique. The unbalanced charge on the top layer will cause a polar cleaved surface.[14] STM and LEED results show that on the surface of $BaFe_{2-x}Co_xAs_2$, the exposed alkaline-earth layer has 1/2 Ba layer and the Ba atoms form a 2×1 or $\sqrt{2}\times\sqrt{2}$ reconstruction[15] and the surface state band will broaden the ARPES peaks and bring uncertainty to the ARPES results on this material.[16] On the other hand, the cleaved surfaces of "111" and "11" families are alkaline metal or FeSe layers, where no unbalanced charge and contribution from the surface state is observed,[15,17] The "111" and "11" families are ideal for ARPES studies.

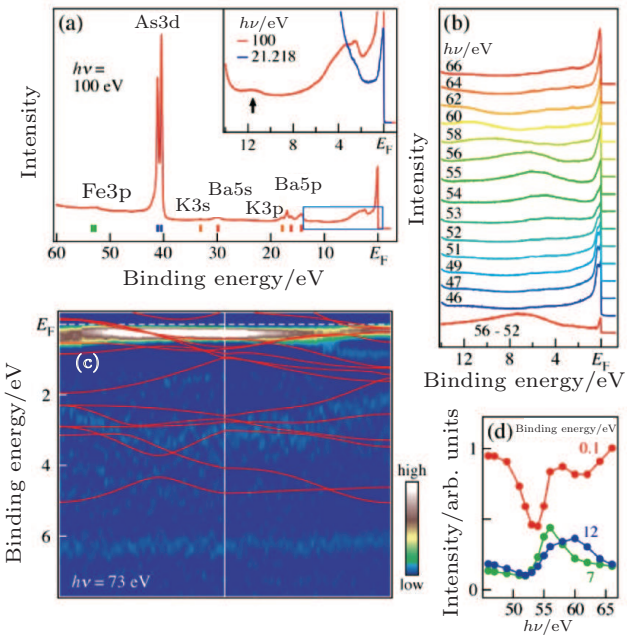


Fig. 4. ARPES spectra of $Ba_{0.6}K_{0.4}Fe_2As_2$ ($T_C = 37$ K). (a) Wide range EDC near Γ showing shallow core levels marked by vertical bars above the x axis. The inset shows the magnified valence band and a possible satellite peak at ~ 12 eV, and highlights the difference between spectra taken at 100 eV and 21.2 eV. (b) Valence band near Γ, measured at different photon energies (46 eV–66 eV). All EDCs are normalized by the photon flux. (c) Intensity plots of second derivatives of spectra along Γ–X and X–M. LDA bands are plotted for comparison. (d) Photon energy dependence of the EDC intensity shown in (b), obtained at binding energies 0.1 eV, 7 eV, and 12 eV. Cited from Ref. [13].

The Angle-resolved photoemission spectroscopy measurement of the hole-doped $Ba_{0.6}K_{0.4}Fe_2As_2$, done by Ding *et al.*[13] shows the typical valence band structure of the IBSCs. The valence band and the near E_F electronic structure of the superconducting $Ba_{0.6}K_{0.4}Fe_2As_2$ are shown in Fig. 4. From Fig. 4(a), the wide energy range EDC shows double peaks at binding energy 40.4 eV and 41.1 eV from the As $3d_{5/2}$ and As $3d_{3/2}$ doublets. Fe 3p (52.4 eV, 53.0 eV), K 3s (33.0 eV), and 3p (17.8 eV), Ba 5s (29.7 eV) and 5p (14.2 eV, 16.2 eV) are also seen and marked. Near the E_F, the state is mainly from Fe 3d orbitals. However, due to the strong correlation effect of the 3d electron predicted by LDA and DMFT results,[18–20] the bands within 2 eV of the E_F are renormalized. From Fig. 4(c), the near E_F structure is renormalized to 1 eV from the LDA predicted range (2 eV), suggesting the strong correlation of electrons in IBSCs.

Close to E_F, the high resolution ARPES measurements are shown in Fig. 5. Several dispersive bands are observed close to E_F. Along the high symmetry lines, Γ–M and Γ–X, the EDC plots and the E versus k intensity plots show three hole-like bands close to the Brillouin zone center (Γ) and two electronic bands at Brillouin zone corner (M), as shown in Figs. 5(a)–5(e). From the LDA calculations,[21] there are three hole-like bands near the Γ point, forming three hole-like FSs, and two electron-like bands near M, forming two electron-like FSs. The LDA calculations need to be normalized by a factor of 2 in order to accord with the measured band dispersion. A similar factor has been observed in "1111"-type iron pnictides.[20] The renormalization factor of 2 implies the importance of the correlation effect in the IBSCs.

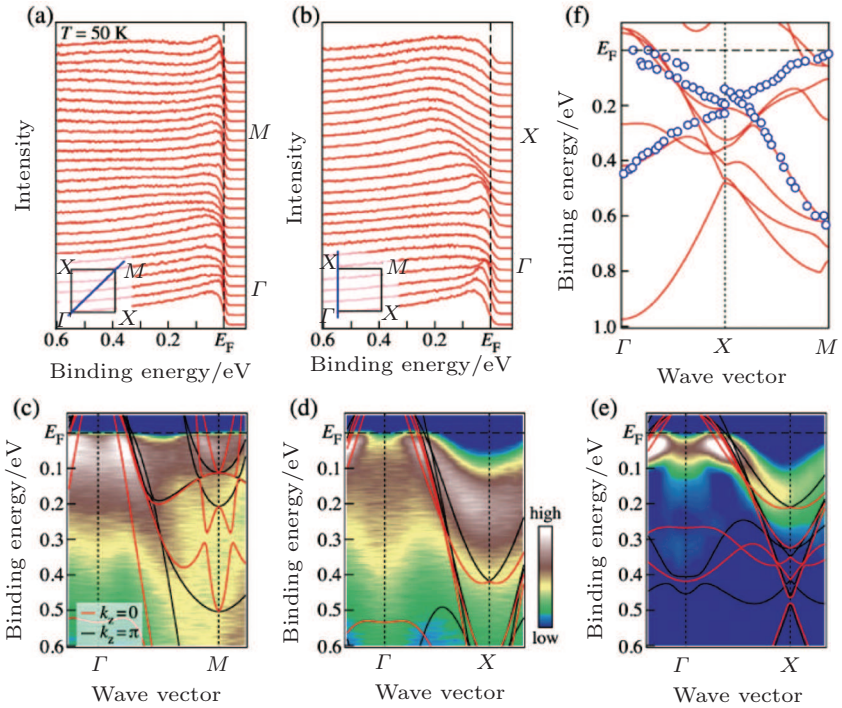


Fig. 5. EDCs measured at 50 K for $Ba_{0.6}K_{0.4}Fe_2As_2$ ($T_C = 37$ K) along (a) Γ–M and (b) Γ–X ($h\nu = 21.2$ eV). Intensity plots of the same spectra along (c) Γ–M and (d) Γ–X. LDA calculated bands at $k_z = 0$ and $k_z = \pi$ are plotted for comparison. (e) Intensity plot of second derivatives of the spectra along Γ–X in comparison with normalized LDA bands (divided by 2). (f) Extracted band positions (circles) measured at 45 eV along Γ–X–M with comparisons to the same normalized LDA bands. Cited from Ref. [13].

5. Band structure of NaFeAs and LiFeAs

The NaFeAs and LiFeAs families have the similar electronic structure to other IBSCs.[22,23] However, there are a few differences between the NaFeAs and LiFeAs superconductors. Compared with the magnetic ground state in "1111" and "122" families,[6,24,25] the NaFeAs has weak magnetic structure with SDW ground state and the LiFeAs is nonmagnetic.[26–29] Structurally, the As–Fe–As angle in NaFeAs is closer to that in "122" system than LiFeAs.[30] ARPES results show that the quasi-particle peaks are sharper in NaFeAs- and LiFeAs-based superconductors than in "122" and "1111" families, which is partially attributed to the non-polar cleaved surface.[28,31–33]

He *et al.*[34] have reported on the ARPES result of NaFeAs, the parent compound of $NaFe_{1-x}Co_xAs$. From the phase diagram shown in Fig. 2, the NaFeAs has three phase transitions while cooling down from high temperature. The transport measurement has shown the transitions and they were identified as structural, magnetic and superconducting transition at 52 K, 41 K, and 23 K.[35] Neutron scattering and NMR measurement confirmed the successive transition. The low temperature ground state has a collinear antiferromagnetic arrangement with orthorhombic structure.[5,36]

The ARPES measurement on NaFeAs by He *et al.*[34] shows that three hole-like bands near BZ center and two electron bands near the BZ corner, the same as in 122 family. At the temperature above the magnetic and structural transitions, as in Figs. 6(a)–6(c), the FSs and the band structure along the high symmetry Γ–M line are simple. Three hole-like bands form two FSs at zone center, while the third band sinks below the Fermi level. When cooling down below the structural and magnetic transition temperatures into the SDW state, the electronic structure undergoes drastic change. At low temperature, three hole-like FSs are observed at the zone center and a cross-like FS is observed at M. An extra hole-like band γ' appeares on the side of other two hole bands due to the folding caused by the SDW state. Close to M, the band is pushed downward caused by collinear magnetic structure and the orthorhombic structure.[37]

The hole band arrangement close to the zone center of LiFeAs is different from the that of NaFeAs. Since the non-magnetic ground state, the SDW and orthorhombic structure observed in NaFeAs do not exist and the electronic structure is purer. ARPES measurement on LiFeAs has also reported on three hole-like bands near the Brillouin zone center and two electronic bands at the zone corner. At low temperature, neither band folding nor splitting was observed in LiFeAs. Figure 7 shows the ARPES measurement of LiFeAs ($T_C \sim 18$ K).[32] The FS topology of the LiFeAs consists of a peanut-like FS at Γ, conventionally called α (and α') FS, a large diamond-like FS (β) also centered at Γ, and two FSs (γ and δ) centered at M. The EDCs along the high symmetry line

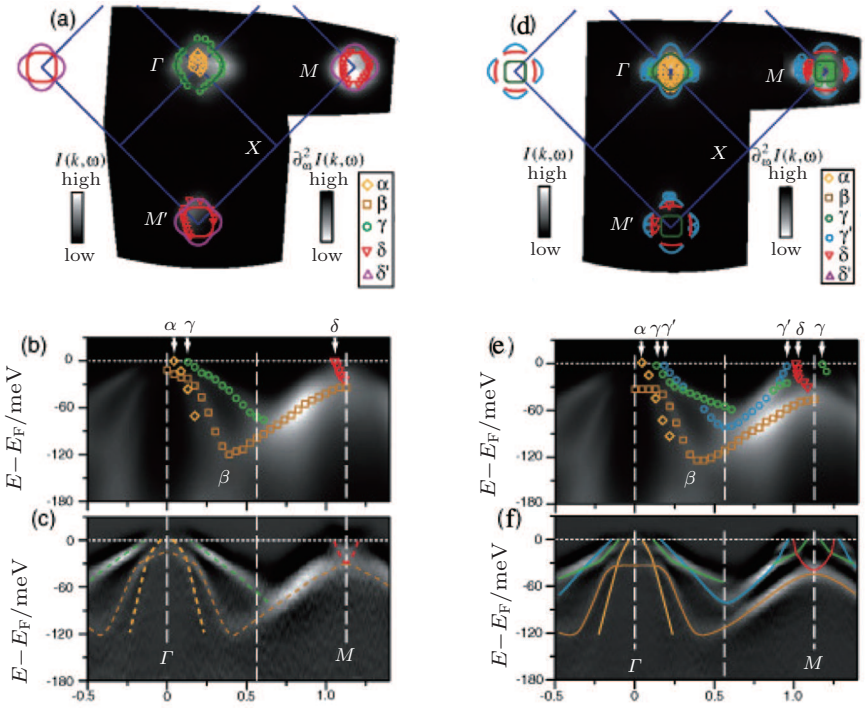


Fig. 6. Electronic structures of NaFeAs at normal state and SDW state. (a) Photoemission intensity map at the E_F integrated over [−5 meV, +5 meV] at normal state; the marks indicate the measured Fermi crossings, the curves are the fitted Fermi surfaces. (b) Photoemission intensity Γ–M direction. (c) The second derivative $[\partial^2_\omega I(k,\omega)]$ for data in (b). (d)–(f) the FS surface topology, intensity, and second derivative of data at SDW state. Cited from Ref. [34].

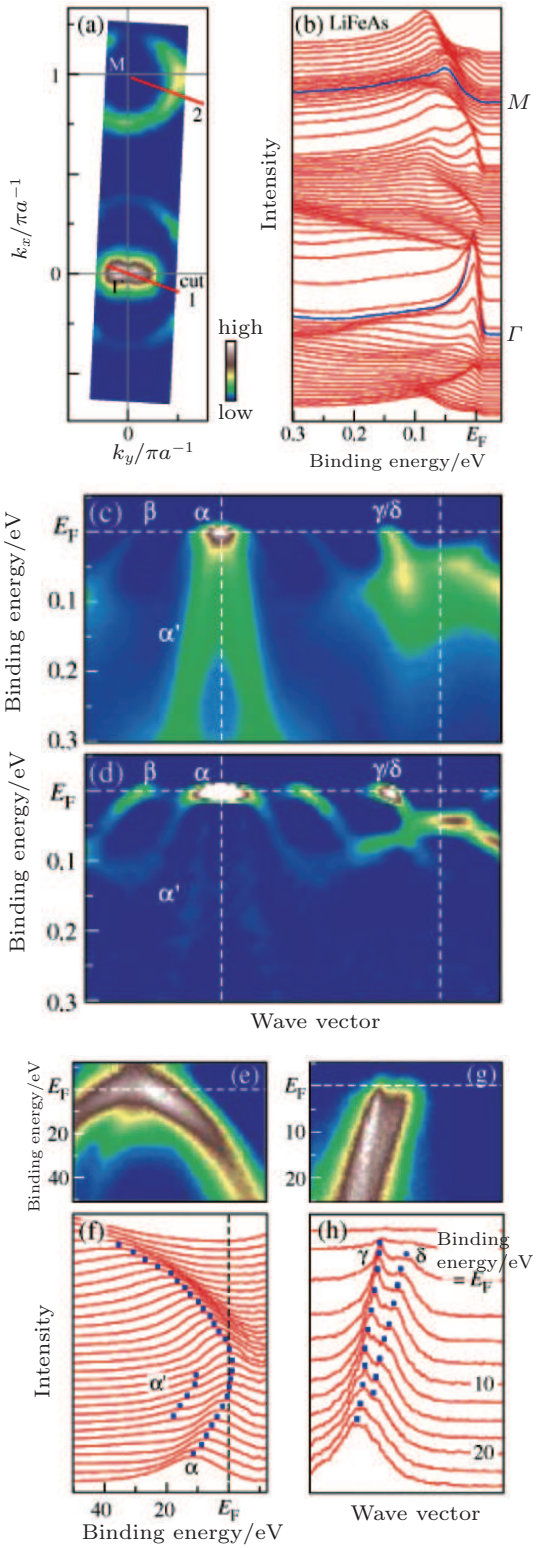


Fig. 7. (a) Plot of the ARPES intensity at E_F of LiFeAs ($T_C \sim 18$ K). The intensity is obtained by integrating the spectra within ± 5 meV with respect to E_F. (b) ARPES spectra along the Γ–M high-symmetry line. (c) and (d) Intensity plot and second-derivative intensity plot of panel (b), respectively, versus binding energy and wave vector. (e) ARPES intensity plot at T $\sim$ 50 K divided by a Fermi–Dirac function measured along cut 1 in panel (a), and (f) corresponding energy distribution curves. (g) ARPES intensity plot at 20 K along the cut 2 and (h) corresponding momentum distribution curves. Dots in panels (f) and (h) are guides for the eye to trace the band dispersion. Cited from Ref. [32]

Γ–M, the corresponding intensity plot, and the second derivative of the intensity plot shown in Figs. 7(b)–7(d) illustrate the dispersions of the bands. In the zone center, there are two hole bands in the vicinity of E_F, with the band tops close to E_F. The more detailed high temperature measurements as shown in Figs. 7(e) and 7(f) show that one hole band (α) crosses the Fermi energy with its band top few meV above E_F, while another hole band (α') is 10 meV below E_F. In between the Γ–M, there exists a large hole band, β, across E_F, forming the large diamond-like FS as shown in Fig. 7(a). At the zone corner, M, two electron bands, γ and δ, are observed, forming two nearly overlapped FSs, as shown in Figs. 7(a), 7(g), and 7(h).

6. Electronic structure of $A_yFe_{2-x}Se_2$

The iron-pnictide has a basic structure of $FeAs_4$ tetrahedron building block. The "11" family has the $FeSe_4$ blocks with the T_C of 8 K,[40] and the T_C could be increased by Te substitution or high pressure up to 37 K.[41–43] The FeSe(Te) has a simpler structure than $FeAs_4$ based superconductor, and there are no atoms in between the FeSe layers. By introducing alkali metal in between FeSe layers, T_C of 30 K was reached in $A_yFe_{2-x}Se_2$.[3] Under high pressure, a second superconducting phase with higher T_C (about 48 K) emerged.[44] Recently, an FeSe monolayer on $SrTiO_3$ substrate showed an indication of T_C above 50 K and possibly up to 77 K.[45]

$A_yFe_{2-x}Se_2$ ($A = K, Rb, Cs, Tl$) are believed to be a heavily electron doped FeSe. However, it turns out that they are exotic materials in structure and electronic structure. The $A_yFe_{2-x}Se_2$ has been discovered with Fe vacancies, and the Fe vacancy forms different orders.[39] Up to now, there has been no consensus on the structure of superconducting phase yet. Bao *et al.*[38] using neutron scattering, discovered a major phase with iron-vacancy order of $\sqrt{5} \times \sqrt{5}$ reconstruction. Yan *et al.*[39] studied the structures and magnetic structures of $A_yFe_{2-x}Se_2$ using TEM and proposed that the superconducting phase is sandwiched between two AFM insulating phases with different Fe vacancy patterns. The phase diagram as function of Fe valance is shown in Fig. 8.

Despite the complexity of the structure, iron-vacancy and the orders, the ARPES measurement on superconducting $A_yFe_{2-x}Se_2$ (A = K, Rb, Cs, Tl) gave consistent results.[46–49] The electronic structure of $K_yFe_{2-x}Se_2$ is qualitatively different from that of the other iron-based superconductors. As shown in Fig. 9, the FS topology of the $K_{0.8}Fe_{1.7}Se_2$ has only the electron-like FSs at BZ corner (M). In the BZ center (Γ), the hole-like bands sink below E_F, no hole-like FS is observed. If we count the enclosed area of the FSs, the $A_yFe_{2-x}Se_2$ can be regarded as heavily electron doped FeSe. Although the vacancy orders have been reported by neutron scattering and TEM, no band folding related to the structural reconstruction was observed, thereby raising a question of the superconducting phase.

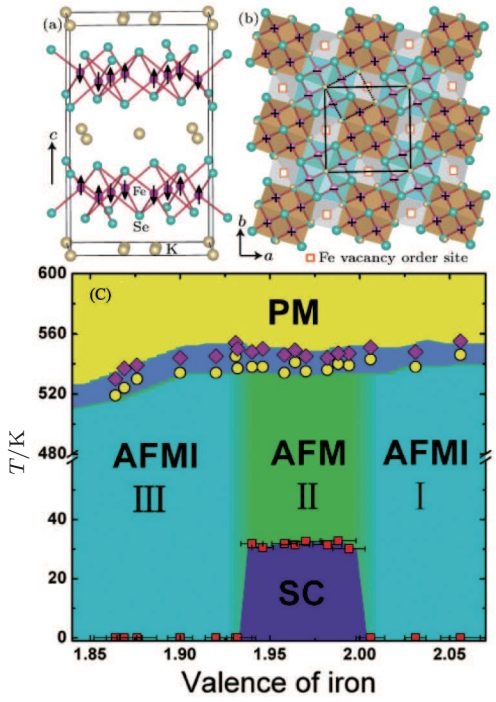


Fig. 8. Crystal and magnetic structures of $K_{0.8}Fe_{1.6}Se_2$ in the low-temperature $I4/m$ unit cell. (a) Crystal structure of $K_{0.8}Fe_{1.6}Se_2$, with magnetic moment orientation. (b) Top view of the top Fe–Se layer. The iron vacancy site Fe(1) is marked by the open square, and the fully occupied Fe(2) site by the circle with the + or – sign indicating magnetic moment direction. The Fe(1) vacancy forms a $\sqrt{5}\times\sqrt{5}$ pattern. (c) Electronic and magnetic phase diagram of $K_xFe_{2-2y}Se_2$ as a function of Fe valence. The phase diagram plotted against the valence of iron. Cited from Refs. [38] and [39].

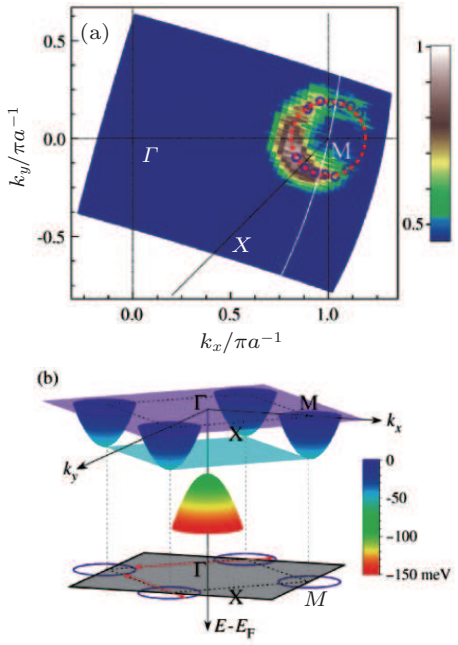


Fig. 9. (a) The angle-resolved photoemission spectroscopy intensity mapping of $K_{0.8}Fe_{1.7}Se_2$ integrated within ±20 meV with respect to E_F. (b) Schematic diagram summarizing the electronic band structure of $K_{0.8}Fe_{1.7}Se_2$. Cited from Ref. [46].

Besides the missing of the hole-FSs, a small electron pocket with strong 3D dispersion is observed at the two-dimensional (2D) BZ center. Photo energy dependent measurement suggested a 3D dispersion near 2D BZ center for the small electron pocket and a 2D-like band dispersion for electron bands near M. Figure 10 shows the FS topologies in Γ and Z planes. The small electron pocket is missing at Γ but visible at Z. In Figs. 10(a) and 10(b), the strong k_z dispersion and a closed FS pocket along k_z are observed. By combining the polarization dependent ARPES measurement and LDA calculation, it is suggested that the small pocket is from the contributions of Fe $3d_{xy}$ and Se $4p_z$ orbitals. Compared with the case of iron-pnictide superconductor, the lowering energy of the Se $4p_z$ orbital may be conducive to both the magnetic superexchange coupling and the superconductivity in iron-chalcogenides.[49]

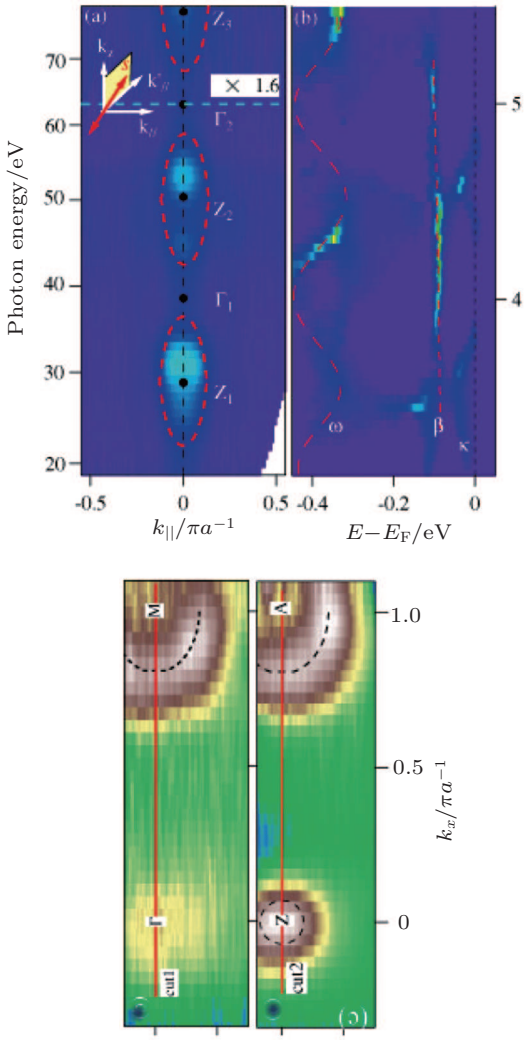


Fig. 10. (a) The angle-resolved photoemission spectroscopy intensity plot in the $h\nu$–$k_{\|}$ plane of $(Tl,Rb)_yFe_{2-x}Se_2$ (±10-meV integration centered at EF). (b) Intensity plot of EDC curvature at $k_{\|}=(0,0)$ with different $h\nu$ values. The band dispersions of the ω and β bands along k_z are indicated by dashed lines serving as guides to the eye. (c) Integrated intensity plots at EF (−10 meV, 10 meV) of (Tl, Rb)$_y$Fe$_{2-x}$Se$_2$ in the Z ($h\nu=28$ eV) and Γ ($h\nu=38$ eV) planes. Cited from Ref. [49].

7. Superconducting gaps and pairing symmetry

The superconducting gap and its symmetry are the keys to the understanding of the pairing mechanism of superconductivity. Compared with the d-wave symmetry of superconducting gap in cuprate high temperature superconductors, the symmetry of the IBSCs is still not fully settled yet. The Knight shift measurement has determined that SC has a spin symmetry of singlet.[50] The difficulties lie in the few aspects: (i) multiple band structures of the IBSCs and the vast IBSC families and (ii) the near-degeneracies of the extended s-wave and d-wave symmetries.[51] Theoretical studies predicted a sign-change s-wave superconductor from the itinerant electrons and the spin-fluctuation modes arising from the nesting across the disconnected electron and hole FSs,[52–54] or short range antiferromagnetic exchange interaction.[55,56]

The IBSCs are regarded as unconventional superconductors because they cannot be explained by the BCS theory. The T_C in IBSC is above the McMillian limit[57] and the large Δ/T_C value implies the IBSC above the weak coupling limit. ARPES measurement indicated that in "111", gaps open on both electron-like and hole-like FSs are both about 5 meV, with $2\Delta/k_BT_C \sim 8$, which is in strong coupling region. Some ARPES measurements indicate smaller gap value in LiFeAs,[31] and proposed that a van Hove singularity is close to E_F as major ingredient to superconductivity, and the difference between ARPES result and STM suggested a large $2\Delta/k_BT_C$ ratio.[32,58] In "122" and "11" families, large ratios of $2\Delta/k_BT_C$ were reported to be in a range of about 7.5–8.[4,59] In the iron-Chalogonides, the nodeless gap size $\Delta \sim 8.5$ meV, which is corresponding to $2\Delta/k_BT_C \sim 7$, is also reported.[47,59–61] Most of the iron based superconductors give large $2\Delta/k_BT_C$ ratio, suggesting that there exists the strong coupling and unconventional superconductivity in this system.

The ARPES measurement of the gap symmetry follows the $s_\pm$ form. Figure 11 shows the gap measurement on different IBSCs with in-plane and out-of-plane gap distributions. From the ARPES data, the general gap symmetry could be fitted by an $s_\pm$ form without plane variation. The in-plane gap distribution on both hole and electron FSs could be fitted to a simple $s_\pm = \Delta_0 \cos k_x \cos k_y$ as shown in Figs. 11(a)–11(e) for $NaFe_{0.95}Co_{0.05}As$ ($T_C = 18$ K), LiFeAs ($T_C = 18$ K) respectively. In addition to the in-plane $s_\pm$ form, the ARPES gap measurement on $Ba_{0.6}K_{0.4}Fe_2As_2$ ($T_C = 37$ K) shows the variation with out-of-plane momentum k_z.[62,63] A fit to the gap size of $Ba_{0.6}K_{0.4}Fe_2As_2$ with consideration of k_z variation, $|\Delta(k_x,k_y,k_z)| = |\Delta_1 \cos k_x \cos k_y + (\Delta_2/2)(\cos k_x \cos k_y)\cos k_z|$, is used and gives the best result as shown in Figs. 11(f)–11(i).[62] A similar result with consideration of k_z variation also gave good fitting to "11" system.[59]

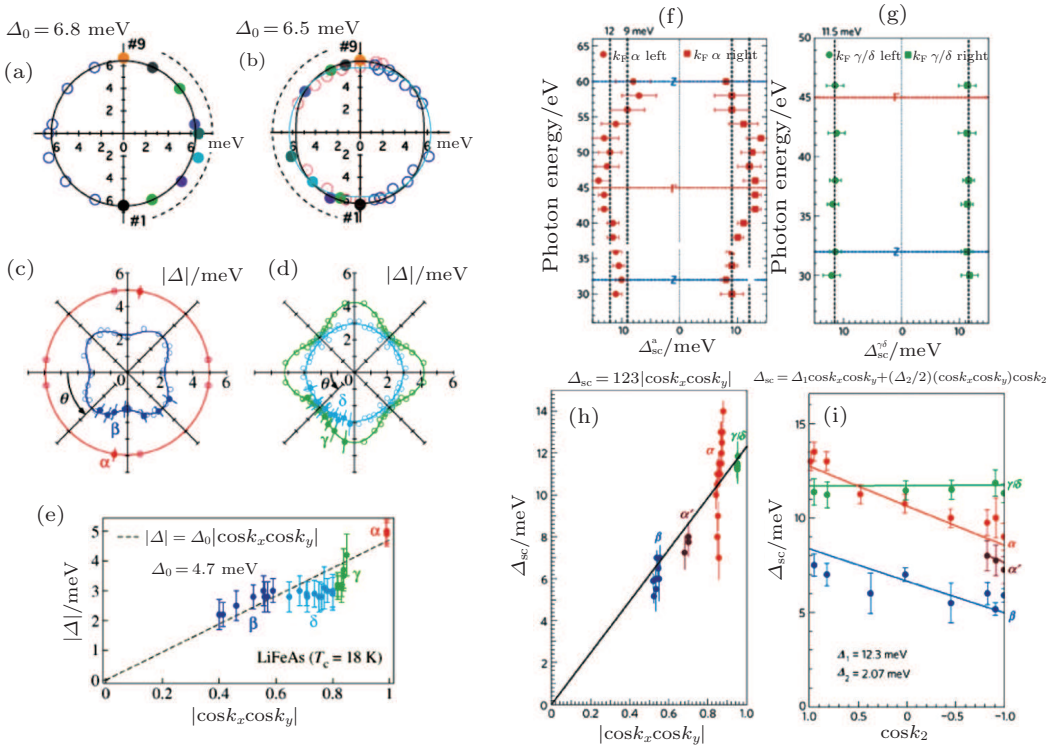


Fig. 11. Gap symmetries of iron-based superconductors. Gap distribution on Co doped $NaFe_{0.95}Co_{0.05}As$ ($T_C = 18$ K) shows isotropic gap distribution on hole (a) and electron (b) Fermi surface. (c) and (d) Gap distributions of LiFeAs ($T_C = 18$ K) as a function of angle and FSs on hole and electron FSs respectively. (e) The $s_\pm$ fitting of gap distribution on LiFeAs. (f) and (g) Gap sizes as a function of photon energy for hole-like band and electron-like band respectively on $Ba_{0.6}K_{0.4}Fe_2As_2$ ($T_C = 37$ K). (h) and (i) $s_\pm$ form fitting of gap symmetry without and with consideration of k_z variation. Panels (a) and (b) are cited from Ref. [33]; panels (c), (d), and (e) are cited from Ref. [32]; panels (f)–(i) are cited from Ref. [62].

In $A_yFe_{2-x}Se_2$, because of the missing of the hole-FSs, only isotropic gaps on electron FSs were reported by various groups.[46–48] Wang *et al.*[64] reported on the ARPES measurement on $Tl_{0.63}K_{0.37}Fe_{1.78}Se_2$ ($T_C = 29$ K) and found only two electron-like FSs at the BZ corner M and the isotropic gaps on that FSs. As shown in Figs. 12(a) and 12(b), two near-degenerate electron-like FSs around M and the gap values are at about 8 meV along the FSs, no indication of node is observed. At the same time, the hole-like bands at zone center sink below E_F. Since there are only two near-degenerate electron FSs observed at M, and the gaps fully open on those FSs, the two electron bands should have no sign-changes,[65,66] an $s_\pm$ form can also be used to fit the gap symmetry of $A_yFe_{2-x}Se_2$.

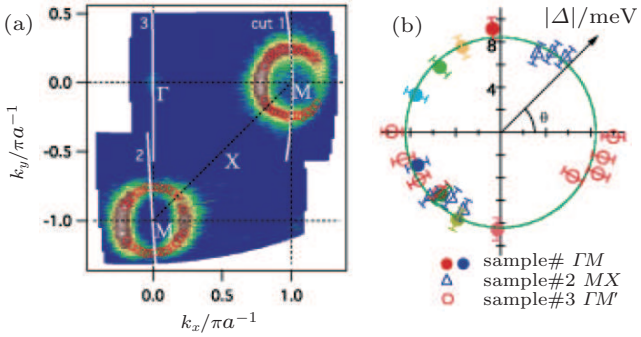


Fig. 12. Gap measurements of superconducting (Tl, K)$Fe_{1.78}Se_2$. (a) Momentum-resolved photoemission intensity mapping of $Tl_{0.63}K_{0.37}Fe_{1.78}Se_2$ recorded in the normal state and integrated over a 10-meV window centred at E_F. (b) Polar distribution of the SC gap size along the FS for 3 different cuts (samples). Cited from Ref. [64].

The theoretical description of the pairing symmetry and pairing mechanism is still not elucidated in IBSCs. Because of the intermediate coupling nature in IBSCs and the existence of five bands near E_F, it is not obvious to start theoretical description.[18,68] From the weak coupling viewpoint, a Fermiology based scenario was proposed.

From the observation of ARPES, the Fermiology found that the "1111", "122", and "11" families gave antiferromagnetic spin fluctuation and created superconducting state. The iron-pnictides share common features of electron and hole FSs. In Figs. 13(a)–13(e), the measurements of superconducting gaps on the superconducting $Ba_{0.6}K_{0.4}Fe_2As_2$ are shown. Gaps on the hole bands (α, β) and two electron bands (γ, δ) are isotropic. No node was observed in this material and most of the IBSCs.[4,69,70] As shown in Fig. 13(f), in $Ba_{0.6}K_{0.4}Fe_2As_2$, one hole-like band (β) and the electron-like band (γ)'s FSs can be connected via a (π, π) vector and both have larger gaps, and another hole-band (α) has a smaller gap and is not nested with any electron bands. A "itinerant" scenario was proposed based on the (quasi)nesting between the hole and electron FSs which will enhance the kinetic process that a zero momentum pair formed on the $\alpha(\gamma)$ FS scattered onto the $\gamma(\alpha)$ FS by the (π, π) fluctuation vector, and the pairing amplitude could be enhanced due to the process. The (π, π) vector is also measured by the neutron scattering experiment.[7,71] The pairing symmetry with the opposite sign on the electron and hole pocket is pairing symmetry for both the electron and hole doped IBSCs.[53,54,68,72]

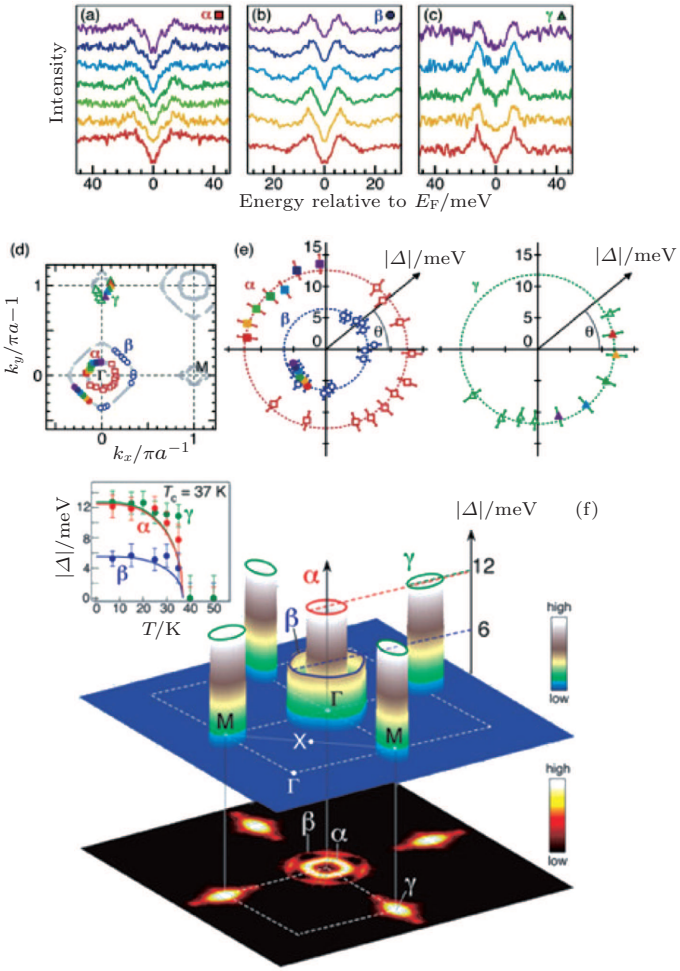


Fig. 13. (a)–(c) Symmetrized EDCs at 15 K on $Ba_{0.6}K_{0.4}Fe_2As_2$ (T_C = 37 K), measured at various k_F points on the α, β, and γ FS, labeled by respective symbols correspondingly. (d) Extracted FS from ARPES measurements in the superconducting state. (e) Superconducting-gap values at 15 K, extracted from the EDCs ((a), (b), and (c)) shown on polar plot for the α, β (left) and γ (right) FS each as a function the of the FS angle. (f) The 3D plot of the superconducting-gap size (Δ) measured at 15 K on the three observed FS sheets (shown at the bottom as an intensity plot) and their temperature evolutions (inset). Cited from Ref. [67].

However, the inter-FS scattering scenario is challenged. In $LiFe_{1-x}Co_xAs$, the highest T_C happens at stoichiometric composition and the ARPES measurement reported on non-nesting of the hole and electron FSs. The missing of the hole-FSs in $A_yFe_{2-x}Se_2$ family posts the great challenge in the scenario. On the inter-FSs scattering, only the nested electron-hole FS pockets as in "11", "111", "122", and "1111" families would lead to a logarithmic divergence in the particle-hole

scattering channel. The material with high T_C (> 30 K) but in the absence of hole-FSs cannot be understood by inter-FS scattering caused pairing scenario.

Besides the pairing mechanism proposed by inter-FS scattering, another candidate is the local magnetic exchange interaction.[55] In IBSCs, the magnetic order is a collinear AF (CAF) state with an ordered wavevector (p, 0)[73] as shown in Fig. 14. This magnetic state of the iron-pnictides can be obtained in a J_1–J_2 Heisenberg model with $J_1 < 2J_2$, where J_1 and J_2 are the nearest neighbor (NN) and the next nearest neighbor (NNN) magnetic exchange interactions. In the iron-chalcognide, the magnetic order state is a bi-collinear AF state with an ordered wave vector $(\pm(\pi/2), \pm(\pi/2))$,[74,75] as shown in Fig. 14(c). $K_{0.8}Fe_{1.6}Se_2$ exhibits a block AF state with an ordered wavevector $(\pm(3\pi/5), \pm(3\pi/5))$.[38] For Fe-chalcognides, the 3rd nearest neighbor term J_3 was included. Neutron scattering measurement found out that all IBSCs share common J_2, which suggests that superconductivity in the iron-pnictides and iron-chalcogenides share a common magnetic origin that is intimately associated with the J_2.[76] By adapting the local antiferromagnetic exchange model, the pairing symmetry of iron pnictides and iron-chalcognides are calculated from the magnetic coupling strength obtained from experimental value and fitted ARPES observation well. In this "strong correlation" paradigm, the effect of electron–electron correlations is very important for high T_C for strengthen local AF exchange interaction. At the same time, the AF exchange interactions can combine with the inter-FS scattering from the "weak coupling" to achieve higher T_C. This scenario covers many common aspects with the cuprate high T_C superconductors.

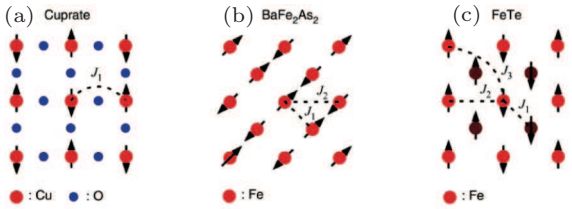


Fig. 14. Magnetically ordered states of HTSCs. (a) Checkerboard AF ordering in cuprate. (b) Collinear AF ordering in ferropnictides. (c) Bicollinear AF ordering in ferrochalcogenides.[55]

8. Summary

The iron-based superconductors have been one of the most important discoveries in recent years. After intensive studies for more than four years, it has been an universally received that the IBSCs belong to the unconventional superconductors and are close to the strong coupling region. The IBSCs have multi orbitals close to the Fermi energy, which participate in the superconductivity. The magnetic orders such as AF magnetic exchange interaction and SDW play an important role in the superconductivity. The gap symmetry determined by ARPES has an $s_{\pm}$ form with a contribution from the out-of-plane component. Albeit the electron and magnetic structure are understood well, the underlying pairing mechanism is still under debate. The "itinerant" or "local" magnetic order as pairing mechanism needs further studying.

References

[1] Kamihara Y, Watanabe T, Hirano M and Hosono H 2008 *J. Am. Chem. Soc.* **130** 3296
[2] Ren Z A, Lu W, Yang J, Yi W, Shen X L, Li Z C, Che G C, Dong X L, Sun L L, Zhou F and Zhao Z X 2008 *Chin. Phys. Lett.* **25** 2215
[3] Guo J, Jin S, Wang G, Wang S, Zhu K, Zhou T, He M and Chen X 2010 *Phys. Rev. B* **82** 180520
[4] Zhao L, Liu H Y, Zhang W T, Meng J Q, Jia X W, Liu G D, Dong X L, Chen G F, Luo J L, Wang N L, Lu W, Wang G L, Zhou Y, Zhu Y, Wang X Y, Xu Z Y, Chen C T and Zhou X J 2008 *Chin. Phys. Lett.* **25** 4402
[5] Li S, de la Cruz C, Huang Q, Chen G F, Xia T L, Luo J L, Wang N L and Dai P 2009 *Phys. Rev. B* **80** 020504
[6] Tucker G S, Fernandes R M, Li H F, Thampy V, Ni N, Abernathy D L, Bud'ko S L, Canfield P C, Vaknin D, Schmalian J and McQueeney R J 2012 *Phys. Rev. B* **86** 024505
[7] Lynn J W and Dai P 2009 *Physica C* **469** 469
[8] Wang X F, Wu T, Wu G, Liu R H, Chen H, Xie Y L and Chen X H 2009 *New J. Phys.* **11** 045003
[9] Wang A F, Luo X G, Yan Y J, Ying J J, Xiang Z J, Ye G J, Cheng P, Li Z Y, Hu W J and Chen X H 2012 *Phys. Rev. B* **85** 224521
[10] Parker D R, Smith M J P, Lancaster T, Steele A J, Franke I, Baker P J, Pratt F L, Pitcher M J, Blundell S J and Clarke S J 2010 *Phys. Rev. Lett.* **104** 057007
[11] Zhou X J, Shi J, Yoshida T, Cuk T, Yang W L, Brouet V, Nakamura J, Mannella N, Komiya S, Ando Y, Zhou F, Ti W X, Xiong J W, Zhao Z X, Sasagawa T, Kakeshita T, Eisaki H, Uchida S, Fujimori A, Zhang Z, Plummer E W, Laughlin R B, Hussain Z and Shen Z X 2005 *Phys. Rev. Lett.* **95** 117001
[12] Hsieh D, Qian D, Wray L, Xia Y, Hor Y S, Cava R J and Hasan M Z 2008 *Nature* **452** 970
[13] Ding H, Nakayama K, Richard P, Souma S, Sato T, Takahashi T, Neupane M, Xu Y M, Pan Z H, Fedorov A V, Wang Z, Dai X, Fang Z, Chen G F, Luo J L and Wang N L 2011 *J. Phys.: Condens. Matter* **23** 135701
[14] Nascimento V B, Li A, Jayasundara D R, Xuan Y, O'Neal J, Pan S, Chien T Y, Hu B, He X B, Li G, Sefat A S, McGuire M A, Sales B C, Mandrus D, Pan M H, Zhang J, Jin R and Plummer E W 2009 *Phys. Rev. Lett.* **103** 076104
[15] Massee F, de Jong S, Huang Y, Kaas J, van Heumen E, Goedkoop J B and Golden M S 2009 *Phys. Rev. B* **80** 140507
[16] van Heumen E, Vuorinen J, Koepernik K, Massee F, Huang Y, Shi M, Klei J, Goedkoop J, Lindroos M, van den Brink J and Golden M S 2011 *Phys. Rev. Lett.* **106** 027002
[17] Zhou X, Cai P, Wang A, Ruan W, Ye C, Chen X, You Y, Weng Z Y and Wang Y 2012 *Phys. Rev. Lett.* **109** 037002
[18] Haule K, Shim J H and Kotliar G 2008 *Phys. Rev. Lett.* **100** 226402
[19] Craco L, Laad M S, Leoni S and Rosner H 2008 *Phys. Rev. B* **78** 134511
[20] Lu D H, Yi M, Mo S K, Erickson A S, Analytis J, Chu J H, Singh D J, Hussain Z, Geballe T H, Fisher I R and Shen Z X 2008 *Nature* **455** 81
[21] Xu G, Zhang H, Dai X and Fang Z 2008 *Europhys. Lett.* **84** 67015
[22] Wang X, Liu Q, Lü Y, Gao W, Yang L, Yu R, Li F and Jin C 2008 *Solid State Commun.* **148** 538
[23] Nekrasov I A, Pchelkina Z V and Sadovskii M V 2008 *JETP Lett.* **88** 543
[24] Zhao J, Huang Q, de la Cruz C, Li S, Lynn J W, Chen Y, Green M A, Chen G F, Li G, Li Z, Luo J L, Wang N L and Dai P 2008 *Nat. Mater* **7** 953
[25] Avci S, Chmaissem O, Chung D Y, Rosenkranz S, Goremychkin E A, Castellan J P, Todorov I S, Schlueter J A, Claus H, Daoud-Aladine A, Khalyavin D D, Kanatzidis M G and Osborn R 2012 *Phys. Rev. B* **85** 184507

[26] Wang M, Wang X C, Abernathy D L, Harriger L W, Luo H Q, Zhao Y, Lynn J W, Liu Q Q, Jin C Q, Fang C, Hu J and Dai P 2011 *Phys. Rev. B* **83** 220515

[27] Taylor A E, Pitcher M J, Ewings R A, Perring T G, Clarke S J and Boothroyd A T 2011 *Phys. Rev. B* **83** 220514

[28] Knolle J, Zabolotnyy V B, Eremin I, Borisenko S V, Qureshi N, Braden M, Evtushinsky D V, Kim T K, Kordyuk A A, Sykora S, Hess C, Morozov I V, Wurmehl S, Moessner R and Buechner B **10** 2012

[29] Ma L, Zhang J, Chen G F and Yu W 2010 *Phys. Rev. B* **82** 180501

[30] Parker D R, Pitcher M J, Baker P J, Franke I, Lancaster T, Blundell S J and Clarke S J 2009 *Chem. Commun.* pp. 2189–2191

[31] Borisenko S V, Zabolotnyy V B, Evtushinsky D V, Kim T K, Morozov I V, Yaresko A N, Kordyuk A A, Behr G, Vasiliev A, Follath R and Büchner B 2010 *Phys. Rev. Lett.* **105** 067002

[32] Umezawa K, Li Y, Miao H, Nakayama K, Liu Z H, Richard P, Sato T, He J B, Wang D M, Chen G F, Ding H, Takahashi T and Wang S C 2012 *Phys. Rev. Lett.* **108** 037002

[33] Liu Z H, Richard P, Nakayama K, Chen G F, Dong S, He J B, Wang D M, Xia T L, Umezawa K, Kawahara T, Souma S, Sato T, Takahashi T, Qian T, Huang Y, Xu N, Shi Y, Ding H and Wang S C 2011 *Phys. Rev. B* **84** 064519

[34] He C, Zhang Y, Xie B P, Wang X F, Yang L X, Zhou B, Chen F, Arita M, Shimada K, Namatame H, Taniguchi M, Chen X H, Hu J P and Feng D L 2010 *Phys. Rev. Lett.* **105** 117002

[35] Chen G F, Hu W Z, Luo J L and Wang N L 2009 *Phys. Rev. Lett.* **102** 227004

[36] Ma L, Chen G F, Yao D X, Zhang J, Zhang S, Xia T L and Yu W 2011 *Phys. Rev. B* **83** 132501

[37] Zhang Y, He C, Ye Z R, Jiang J, Chen F, Xu M, Ge Q Q, Xie B P, Wei J, Aeschlimann M, Cui X Y, Shi M, Hu J P and Feng D L 2012 *Phys. Rev. B* **85** 085121

[38] Bao W, Huang Q Z, Chen G F, Green M A, Wang D M, He J B and Qiu Y M 2011 *Chin. Phys. Lett.* **28** 086104

[39] Yan Y J, Zhang M, Wang A F, Ying J J, Li Z Y, Qin W, Luo X G, Li J Q, Hu J and Chen X H 2012 *Sci. Rep.* **2** 212

[40] Hsu F C, Luo J Y, Yeh K W, Chen T K, Huang T W, Wu P M, Lee Y C, Huang Y L, Chu Y Y, Yan D C and Wu M K 2008 *Proc. Natl. Acad. Sci. USA* **105** 14262

[41] Fang M H, Pham H M, Qian B, Liu T J, Vehstedt E K, Liu Y, Spinu L and Mao Z Q 2008 *Phys. Rev. B* **78** 224503

[42] Yeh K W, Huang T W, Huang Y l, Chen T K, Hsu F C, Wu P M, Lee Y C, Chu Y Y, Chen C L, Luo J Y, Yan D C and Wu M K 2008 *Europhys. Lett.* **84** 37002

[43] Margadonna S, Takabayashi Y, Ohishi Y, Mizuguchi Y, Takano Y, Kagayama T, Nakagawa T, Takata M and Prassides K 2009 *Phys. Rev. B* **80** 064506

[44] Sun L, Chen X J, Guo J, Gao P, Huang Q Z, Wang H, Fang M, Chen X, Chen G, Wu Q, Zhang C, Gu D, Dong X, Wang L, Yang K, Li A, Dai X, Mao H K and Zhao Z 2012 *Nature* **483** 67

[45] Wang Q Y, Li Z, Zhang W H, Zhang Z C, Zhang J S, Li W, Ding H, Ou Y B, Deng P, Chang K, Wen J, Song C L, He K, Jia J F, Ji S H, Wang Y Y, Wang L L, Chen X, Ma X C and Xue Q K 2012 *Chin. Phys. Lett.* **29** 057004

[46] Qian T, Wang X P, Jin W C, Zhang P, Richard P, Xu G, Dai X, Fang Z, Guo J G, Chen X L and Ding H 2011 *Phys. Rev. Lett.* **106** 187001

[47] Zhang Y, Yang L X, Xu M, Ye Z R, Chen F, He C, Xu H C, Jiang J, Xie B P, Ying J J, Wang X F, Chen X H, Hu J P, Matsunami M, Kimura S and Feng D L 2011 *Nat. Mater.* **10** 273

[48] Mou D, Liu S, Jia X, He J, Peng Y, Zhao L, Yu L, Liu G, He S, Dong X, Zhang J, Wang H, Dong C, Fang M, Wang X, Peng Q, Wang Z, Zhang S, Yang F, Xu Z, Chen C and Zhou X J 2011 *Phys. Rev. Lett.* **106** 107001

[49] Liu Z H, Richard P, Xu N, Xu G, Li Y, Fang X C, Jia L L, Chen G F, Wang D M, He J B, Qian T, Hu J P, Ding H and Wang S C 2012 *Phys. Rev. Lett.* **109** 037003

[50] Grafe H J, Paar D, Lang G, Curro N J, Behr G, Werner J, Hamann-Borrero J, Hess C, Leps N, Klingeler R and Büchner B 2008 *Phys. Rev. Lett.* **101** 047003

[51] Graser S, Maier T A, Hirschfeld P J and Scalapino D J 2009 *New J. Phys.* **11** 025016

[52] Kuroki K, Onari S, Arita R, Usui H, Tanaka Y, Kontani H and Aoki H 2008 *Phys. Rev. Lett.* **101** 087004

[53] Mazin I I, Singh D J, Johannes M D and Du M H 2008 *Phys. Rev. Lett.* **101** 057003

[54] Chubukov A V, Efremov D V and Eremin I 2008 *Phys. Rev. B* **78** 134512

[55] Hu J and Ding H 2012 *Sci. Rep.* **2** 381

[56] Wysocki A L, Belashchenko K D and Antropov V P 2011 *Nat. Phys.* **7** 485

[57] Chen X H, Wu T, Wu G, Liu R H, Chen H and Fang D F 2008 *Nature* **453** 761

[58] Allan M P, Rost A W, Mackenzie A P, Xie Y, Davis J C, Kihou K, Lee C H, Iyo A, Eisaki H and Chuang T M 2012 *Science* **336** 563

[59] Miao H, Richard P, Tanaka Y, Nakayama K, Qian T, Umezawa K, Sato T, Xu Y M, Shi Y B, Xu N, Wang X P, Zhang P, Yang H B, Xu Z J, Wen J S, Gu G D, Dai X, Hu J P, Takahashi T and Ding H 2012 *Phys. Rev. B* **85** 094506

[60] Chen F, Xu M, Ge Q Q, Zhang Y, Ye Z R, Yang L X, Jiang J, Xie B P, Che R C, Zhang M, Wang A F, Chen X H, Shen D W, Hu J P and Feng D L 2011 *Phys. Rev. X* **1** 021020

[61] Wang X P, Richard P, van Roekeghem A, Huang Y B, Razzoli E, Qian T, Wang H D, Dong C H, Fang M H, Shi M and Ding H 2012 arXiv: 1205.0996v1[cond-mat]

[62] Xu Y M, Huang Y B, Cui X Y, Razzoli E, Radovic M, Shi M, Chen G F, Zheng P, Wang N L, Zhang C L, Dai P C, Hu J P, Wang Z and Ding H 2011 *Nat. Phys.* **7** 198

[63] Nakayama K, Sato T, Richard P, Xu Y M, Sekiba Y, Souma S, Chen G F, Luo J L, Wang N L, Ding H and Takahashi T 2009 *Europhys. Lett.* **85** 67002

[64] Wang X P, Qian T, Richard P, Zhang P, Dong J, Wang H D, Dong C H, Fang M H and Ding H 2011 *Europhys. Lett.* **93** 57001

[65] Zhou Y, Xu D H, Zhang F C and Chen W Q 2011 *Europhys. Lett.* **95** 17003

[66] Saito T, Onari S and Kontani H 2010 *Phys. Rev. B* **82** 144510

[67] Ding H, Richard P, Nakayama K, Sugawara K, Arakane T, Sekiba Y, Takayama A, Souma S, Sato T, Takahashi T, Wang Z, Dai X, Fang Z, Chen G F, Luo J L and Wang N L 2008 *Europhys. Lett.* **83** 47001

[68] Wang F, Zhai H, Ran Y, Vishwanath A and Lee D H 2009 *Phys. Rev. Lett.* **102** 047005

[69] Evtushinsky D V, Zabolotnyy V B, Harnagea L, Yaresko A N, Thirupathaiah S, Kordyuk A A, Maletz J, Aswartham S, Wurmehl S, Rienks E, Follath R, Büchner B and Borisenko S V 2013 *Phys. Rev. B* **87** 094501

[70] Okazaki K, Ito Y, Ota Y, Kotani Y, Shimojima T, Kiss T, Watanabe S, Chen C T, Niitaka S, Hanaguri T, Takagi H, Chainani A and Shin S 2012 *Phys. Rev. Lett.* **109** 237011

[71] Lumsden M D and Christianson A D 2010 *J. Phys.: Condens. Matter* **22** 20

[72] Raghu S, Qi X L, Liu C X, Scalapino D J and Zhang S C 2008 *Phys. Rev. B* **77** 220503

[73] de la Cruz C, Huang Q, Lynn J W, Li J Y, Ratcliff W, Zarestky J L, Mook H A, Chen G F, Luo J L, Wang N L and Dai P C 2008 *Nature* **453** 899

[74] Bao W, Qiu Y, Huang Q, Green M A, Zajdel P, Fitzsimmons M R, Zhernenkov M, Chang S, Fang M, Qian B, Vehstedt E K, Yang J, Pham H M, Spinu L and Mao Z Q 2009 *Phys. Rev. Lett.* **102** 247001

[75] Li S, de la Cruz C, Huang Q, Chen Y, Lynn J W, Hu J, Huang Y L, Hsu F C, Yeh K W, Wu M K and Dai P 2009 *Phys. Rev. B* **79** 054503

[76] Lipscombe O, Chen G, Fang C, Perring T, Abernathy D, Christianson A, Egami T, Wang N L, Hu J P and Dai P C 2011 *Phys. Rev. Lett.* **106** 057004